



ELSEVIER

Journal of Nuclear Materials 313–316 (2003) 1066–1070

**journal of
nuclear
materials**

www.elsevier.com/locate/jnucmat

Neutral transport simulations of gas puff imaging experiments

 D.P. Stotler ^{a,*}, B. LaBombard ^b, J.L. Terry ^b, S.J. Zweben ^a
^a Princeton Plasma Physics Laboratory, Princeton University, P.O. Box 451, Princeton, NJ 08543-0451, USA

^b MIT Plasma Science and Fusion Center, NW17, Cambridge, MA 02139, USA

Received 27 May 2002; accepted 12 September 2002

Abstract

Visible imaging of gas puffs has been used on the Alcator C-Mod tokamak to characterize edge plasma turbulence, yielding data that can be compared with plasma turbulence codes. Simulations of these experiments with the DEGAS 2 Monte Carlo neutral transport code have been carried out to explore the relationship between the plasma fluctuations and the observed light emission. By imposing two-dimensional modulations on the measured time-average plasma density and temperature profiles, we demonstrate that the spatial structure of the emission cloud reflects that of the underlying turbulence. However, the photon emission rate depends on the plasma density and temperature in a complicated way, and no simple scheme for inferring the plasma parameters directly from the light emission patterns is apparent. The simulations indicate that excited atoms generated by molecular dissociation are a significant source of photons, further complicating interpretation of the gas puff imaging results.

© 2003 Elsevier Science B.V. All rights reserved.

PACS: 52.25.Ya; 52.70.-m; 52.35.Ra

Keywords: Turbulence; Neutral gas modeling; DEGAS code

1. Introduction

The edge plasma of the tokamak is ideal for a comprehensive study of plasma turbulence. First, the relatively low electron densities and temperatures as well as the location make the edge plasma accessible to study with reciprocating probes. Second, the low temperatures also allow atomic physics processes to be used as the basis for diagnostics. The potential benefit of understanding turbulence in the edge plasma is great since the boundary conditions for the core plasma are set in or near this region.

The gas puff imaging (GPI) diagnostic [1–3] is designed to exploit these prospects and to provide two-

dimensional (2-D) data on the structure of the plasma turbulence for comparison with three-dimensional (3-D) nonlinear plasma simulation codes and with direct probe measurements of the turbulence characteristics. The GPI diagnostic consists of recording with high temporal and spatial resolution [1] the light generated by neutral atoms puffed into the edge of the plasma. The experiments considered in this paper use deuterium as the working gas.

The relationship between the camera images and the underlying plasma fluctuations can be explored in a straightforward way with the Monte Carlo neutral transport code DEGAS 2 [4]. The number of molecules puffed is small enough to not significantly perturb the plasma [1]. Yet, the emitted light is much brighter than that arising from background neutral species [1]. Hence, the latter need not be simulated. Because the neutrals come from a gas puff rather than the recycling of plasma ions, interactions of the neutral species with material surfaces should not be important.

* Corresponding author. Tel.: +1-609 243 2063; fax: +1-609 243 2662.

E-mail address: dstotler@pppl.gov (D.P. Stotler).

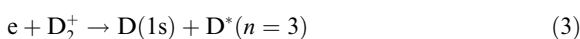
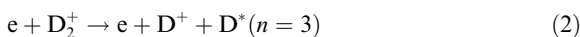
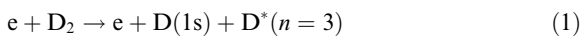
2. Description of simulations

The Alcator C-Mod geometry used in DEGAS 2 is built up from a simple outline of the vacuum vessel, including the gas puff nozzle and surrounding structures, and an equilibrium computed for the shot and time of interest. A 2-D plasma mesh is established using the DG and CARRE packages [5]. The volume between the plasma mesh and the material surfaces is broken up into triangles [6]. The mesh zones in the emission region have linear dimensions on the order of a few millimeters. The input geometry and plasma data are toroidally symmetric.

The GPI experiments survey the radial and poloidal structure of the plasma turbulence by using camera viewing chords oriented along the magnetic field [1]. The present version of DEGAS 2 is not set up to resolve the light emission in 3-D, as would be needed for quantitative comparisons of photon intensity. Instead, the code results are effectively toroidally averaged to yield 2-D profiles of the Balmer- α (D_α) intensity in the poloidal plane that can be compared qualitatively with the experimental data. The radial D_α profile obtained from a preliminary (i.e., without molecular contributions) simulation [1] is sufficiently similar to the time-average experimental result that we are confident that the conclusions of this work are pertinent to the experimental situation. Toroidal resolution will be added in future work, and the GPI camera views will be modeled directly. This will allow a quantitative comparison of the image intensity and an evaluation of the spatial averaging caused by the finite toroidal extent of the emission cloud.

These DEGAS 2 simulations are time-independent. The radiative decay time of the upper level of the emitting transition (principal quantum number $n = 3$) is $<0.02 \mu\text{s}$, much shorter than the autocorrelation time for the turbulence of $10\text{--}20 \mu\text{s}$ [1]. The time required for a 3 eV (a typical dissociation energy) atom to cross the emission cloud is about $1 \mu\text{s}$, also short enough for the steady state assumption to be valid. Time-dependent neutral transport will be investigated in subsequent work.

The deuterium atomic and molecular physics processes incorporated into these simulations have been described elsewhere [7,8]. Balmer- α photons resulting from D_2 and D_2^+ dissociation are included using the reactions:



The rates and kinetics of these processes are discussed in Ref. [8]. Neutral-neutral collisions are not included in

these simulations, even though they may not be negligible. To treat them correctly, we would need a realistic value for the neutral densities and, hence, a toroidally resolved calculation modeling the 3-D expansion of the gas flowing away from the nozzle.

The emission rate of the observed light in $\text{m}^{-3} \text{s}^{-1}$ is computed by an expression equivalent to

$$S_{D_\alpha} = \sum_{j=D, D_2, D_2^+} n_j f_j(n_e, T_e), \quad (4)$$

where n_j is the computed density of the electronic ground state atom, molecule or molecular ion, n_e is the electron density, and T_e is the electron temperature. The function f_D is the ratio of the density of the upper level of the radiative transition to the ground state density times the rate of spontaneous decay (Einstein coefficient) for the transition. The local distribution of neutral atoms over the electronically excited states is obtained from a collisional radiative model (see, for example, Ref. [9]) based on that described in Ref. [10] and utilizing the cross sections of Ref. [11]. The model results are read into DEGAS 2 as tabular data. The relationship between the plasma fluctuations and the light intensity is dominated by the n_e and T_e dependence of f_D .

Note that in DEGAS 2, D_2^+ ions are assumed to be dissociated instantaneously upon being created. As a result, the D_2^+ density is effectively equal to the D_2 density times its ionization rate divided by the D_2^+ destruction rate. The values of f_{D_2} and $f_{D_2^+}$ are given by

$$f_{D_2} = n_e \frac{A_{32}}{A_{31} + A_{32}} \langle \sigma v \rangle_1, \quad (5)$$

$$f_{D_2^+} = n_e \frac{A_{32}}{A_{31} + A_{32}} [\langle \sigma v \rangle_2 + \langle \sigma v \rangle_3], \quad (6)$$

where A_{ij} is the Einstein coefficient for the transition from $n = i$ to $n = j$, and $\langle \sigma v \rangle_k$ is the reaction rate [8] for the k th process with k referring to Eqs. (1)–(3) above.

Time-average radial profiles of the plasma density and temperature are provided by a midplane reciprocating probe. The data are mapped onto the DEGAS 2 mesh by assuming that the density and temperature are constant on a flux surface with ion density $n_i = n_e$ and ion temperature $T_i = T_e$. In the triangulated region of the computational mesh, the radial coordinate is estimated as the physical distance between the zone center and the nearest zone of the flux surface-based mesh.

3. Results

The simulations described here are based on Alcator C-Mod shot 1010622006 at 700 ms. Over the emission region, T_e varies between 10 and 60 eV; n_e ranges from 1×10^{19} to $8 \times 10^{19} \text{ m}^{-3}$. The D_α emission pattern

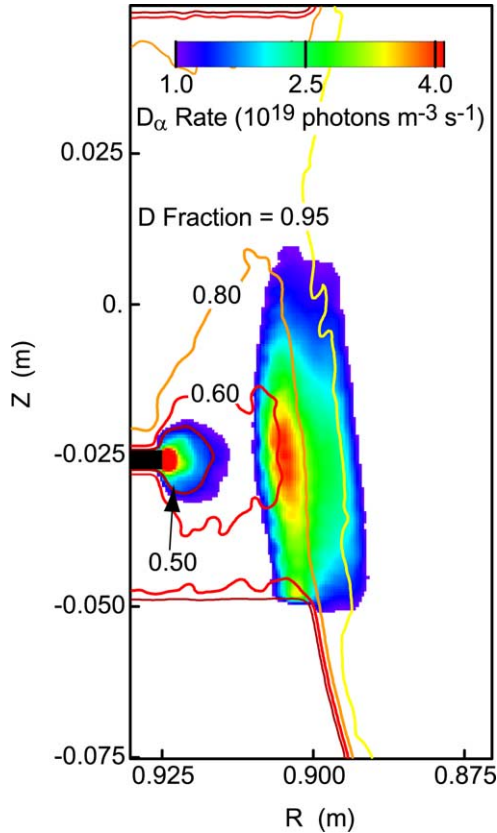


Fig. 1. Balmer- α emission pattern from the baseline DEGAS 2 simulation using the time-average profiles measured by the reciprocating probe. The gas puff nozzle is indicated in black. The contour lines give the fraction of D_α photons due to atoms.

computed from the time-average plasma profiles is shown in Fig. 1.

The small emission peak directly in front of the gas nozzle is not observed experimentally. Its absence in the experiments probably implies that the plasma parameters used in that region are incorrect. Namely, the probe data extend only out to a major radius of $R = 0.91$ m for this shot and are assumed constant at larger radii. The magnitude of this peak would be reduced by more than two orders of magnitude if $T_e < 2.5$ eV or if $n_e < 3.6 \times 10^{16} \text{ m}^{-3}$ at the nozzle. Both possibilities are consistent with an exponential extrapolation of the outermost probe data points. This peak will be ignored in subsequent discussions.

The contours in Fig. 1 indicate the fraction of the photons due to D atoms, $n_D f_D / S_{D_\alpha}$. Note that molecular processes contribute roughly 40% of the photons at the peak of the primary cloud, a much larger fraction than had been expected. An effort should be made to verify this result experimentally.

We investigate the relationship between the instantaneous plasma profiles and the observed emission pat-

terns by imposing on the time-average electron (and ion) density and temperature ad hoc density and temperature modulations,

$$n'_e(R, Z) = n_e(R, Z) \left[1 + \frac{1}{2} \sin\left(\frac{\pi Z}{0.01}\right) \right] \times \left\{ 1 + \frac{1}{2} \sin\left[\frac{\pi(R - R_{\text{sep}} + 0.0035)}{0.005}\right] \right\}, \quad (7)$$

where Z is the height above midplane and R_{sep} is the major radius of the separatrix at midplane. This results in a 0.02 m wavelength for the poloidal variation [1]. The smaller radial wavelength of 0.01 m allows a full period of the modulation to fit inside the emission cloud. The radial shift of 0.0035 m permits the innermost density point to have the same value as in the unperturbed case. The resulting 2-D emission contours are shown in Fig. 2(a). In a separate run, we apply the same perturbation to the electron and ion temperatures; the temperatures are constrained to be between 5 and 100 eV. The effect of the T_i perturbation is expected to be small since T_i only enters through the neutral-ion elastic scattering processes. Fig. 3 shows the D_α intensities from these two runs, both normalized to the unperturbed result, along a vertical slice through the emission clouds. The radius of the slice, $R = 0.904$ m, has been chosen to pass through a peak in the radial variation of Eq. (7).

The simulated emission patterns show the same 2-D structure as the underlying density (or temperature) perturbation. Hence, we anticipate that a poloidal analysis of the experimentally observed emission pattern will yield a spectrum that is at least similar to that of the underlying turbulence. Note that we expect the auto-correlation functions and frequency spectra computed from the GPI images to also mirror those of the plasma. Subsequent investigations will attempt to quantitatively verify these assertions.

The magnitude of the maxima of the normalized D_α quantities in Fig. 3 are smaller than those of the applied modulations largely because $\partial \ln f_D / \partial \ln T_e$ and $\partial \ln f_D / \partial \ln n_e < 1$. In fact, the value of $\partial \ln f_D / \partial \ln T_e$ varies between 0.3 at $R = 0.89$ m and 1.4 at $R = 0.91$ m. Likewise, $\partial \ln f_D / \partial \ln n_e$ rises from 0.5 to 0.8 over the same radial range. At the D_α peak, $R = 0.905$ m, $\partial \ln f_D / \partial \ln T_e = 0.7$ and $\partial \ln f_D / \partial \ln n_e = 0.6$.

The structure of Fig. 3 and the relationship between the normalized modulation and emission amplitudes are more complicated than those displayed in the analogous figure of Ref. [1] due to the molecular contributions to Eq. (4). The density dependencies of f_{D_2} Eq. (5) and $f_{D_2^+}$ Eq. (6) are explicitly linear. Because three different processes contribute to these functions and because of the strong correlation between n_D and n_{D_2} , the temperature dependencies of the molecular contributions to Eq. (4) are complicated. Like f_D , their effective temperature scaling will vary radially.

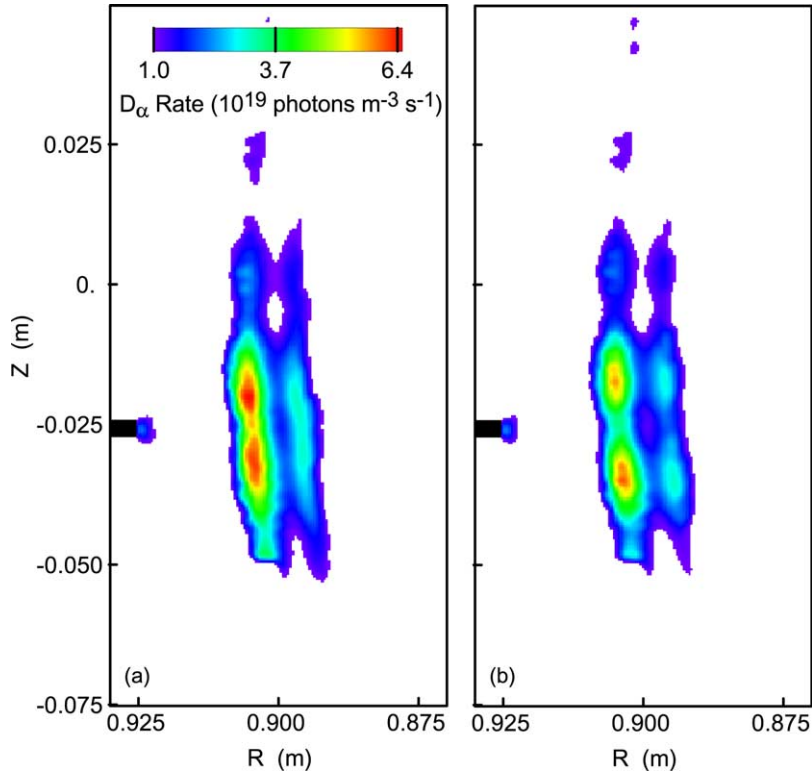


Fig. 2. Balmer- α emission patterns from DEGAS 2 simulation with the electron density perturbation (Eq. (7)). The frame labeled (a) is the result produced directly by the code and, thus, incorporates the ‘shadowing’ effect of the perturbation on the neutral densities. Frame (b) has been assembled in post-processing to eliminate the shadowing effect. Both plots are drawn using the scale shown in (a).

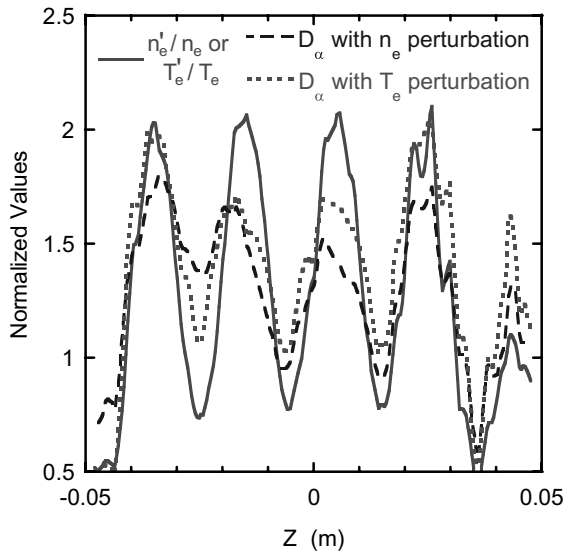


Fig. 3. Vertical variation of the applied plasma parameter modulation (Eq. (7)) and the resulting D_{α} emission patterns normalized to the values obtained in the baseline simulation. This vertical slice is taken at $R = 0.904$ m.

The simplest interpretation of the GPI technique is that the emission patterns primarily reflect electron density fluctuations and that the emission rate is insensitive to temperature fluctuations. This would be valid if $n_e \lesssim 10^{18} \text{ m}^{-3}$ and $T_e \gg 10 \text{ eV}$. However, the Alcator C-Mod edge typically has much higher densities and temperatures not much greater than 10 eV. As has been demonstrated in the last two paragraphs, the density and temperature dependencies of the emission rate are not very different. In particular, they are not sufficiently different to allow the perturbed plasma density or temperature to be inferred directly from the GPI images. Inversion of the data would be simpler if the electron density and temperature perturbations were in phase, as some theories predict.

The preceding arguments have assumed that the neutral density profile in the emission cloud is smooth in comparison with the plasma profiles [1]. In the same way that the edge plasma can affect beam emission spectroscopy [12], localized n_e or T_e fluctuations can modify the flow of GPI neutrals to smaller R via ionization, dissociation, and the other neutral-plasma interaction channels. Alternatively, we can imagine these processes

transferring some of the structure of the plasma turbulence to the neutral density. The neutral density, and thus the light intensity, at those radii will depend on the plasma parameters that have been ‘seen’ by those molecules and atoms en route from the gas nozzle.

To demonstrate this effect, we consider the unperturbed simulation (Fig. 1) and the simulation employing the perturbed n_e profile Fig. 2(a). We can artificially assemble an idealized (i.e., without this effect) emission pattern for the perturbed case using the perturbed f_j obtained from the latter simulation and the unperturbed n_j from the former; the result is shown in Fig. 2(b). Fig. 2(b) reflects more clearly the structure of the imposed n_e perturbation than does Fig. 2(a). In Fig. 2(a), the neutral densities are smaller just behind (i.e., at slightly lower R) the n_e peaks than in the unperturbed case; this behavior has been described as ‘shadowing’. However, the neutral densities are *increased* behind n_e minima. The net result is that the spatial structure of the emission profile in Fig. 2(a) is smeared out relative to the idealized result shown in Fig. 2(b) and relative to that of the perturbed n_e (see also Fig. 3).

To quantify the effect, we normalize the difference of these two images to the unperturbed emission rate:

$$F_s = \left[\sum_j (n'_j - n_j) f'_j \right] / \sum_j n_j f_j. \quad (8)$$

The primes indicate the value obtained with perturbed plasma parameters. We have computed F_s for both of the simulations with perturbed plasma parameters.

Space does not permit 2-D plots of F_s to be shown or explained in detail. Instead, we note only that $|F_s| \gtrsim 0.5$ over a significant area and that most of this is due to the molecular contributions. The cause is a greater sensitivity of the molecular density to the plasma parameters.

In contrast, the analogous shadowing fraction based on the photons from D alone varies between -0.2 and 0.2 over the emission region. The absence of strong interactions between the atoms and the plasma is further confirmed when we examine the physical processes that determined the simulated atom velocities in this region. Namely, each particle in DEGAS 2 has a label that initially points to the type of source that gave rise to the particle (e.g., a gas puff). Upon a collision, the label changes to indicate the reaction responsible (e.g., charge

exchange). The neutral density profile can be broken up into the various contributions made by these processes. The fraction due to charge exchange is less than 0.5 in the region of interest. Only 10–20% have undergone reflection at a material surface. Thus, most of the D emission comes from atoms that have traveled ballistically since being created by a dissociation event.

We conclude that quantitatively interpreting the GPI images will require not only taking into account the density and temperature dependencies of the f_j functions of Eq. (4), but also the effect of the plasma fluctuations on the neutral densities. Neutral transport codes such as DEGAS 2 can facilitate these interpretations, but careful benchmarks of the atomic and molecular models in the code will have to be carried out first. Such simulations will be the subject of a subsequent paper.

Acknowledgements

The authors would like to acknowledge fruitful discussions with R.J. Maqueda. This work was supported by US DOE Contracts DE-AC02-CH03073 and DE-FC02-99ER54512. This work was supported by US DOE Contracts DE-AC02-76CH03073 and DE-FC02-99ER54512.

References

- [1] S.J. Zweben et al., Phys. Plasmas 9 (2002) 1981.
- [2] R.J. Maqueda et al., Rev. Sci. Instrum., will appear in March 2003.
- [3] J.L. Terry et al., J. Nucl. Mater. 290–293 (2001) 757.
- [4] D.P. Stotler, C.F.F. Karney, Contribution Plasma Phys. 34 (1994) 392.
- [5] D.P. Coster, private communication, 1999.
- [6] J.R. Shewchuk, in: M.C. Lin, D. Manocha (Eds.), Applied Computational Geometry: Towards Geometric Engineering, vol. 1148, Springer, New York, 1996, p. 203.
- [7] D.P. Stotler et al., J. Nucl. Mater. 290–293 (2001) 967.
- [8] D.P. Stotler et al., Phys. Plasmas 3 (1996) 4084.
- [9] L.C. Johnson, E. Hinnov, J. Quantum Spectrosc. Radiat. Transfer 13 (1973) 333.
- [10] J.C. Weisheit, J. Phys. B 8 (1975) 2556.
- [11] R.K. Janev, J.J. Smith, At. Plasma-Mater. Interact. Data Fus. 4 (1993) 1, supplement to the J. Nucl. Fus.
- [12] T.A. Gianakon et al., Rev. Sci. Instrum. 63 (1992) 4931.